https://doi.org/10.1590/jatm.v16.1347 ORIGINAL PAPER

Aerodynamic Performance of NACA 66_2-015 Airfoil with Gurney Flap

Balram Mandal[1], Roshani Kumari Gupta[1], Abhinav Adhikari[1], Biranchi Narayana Das[1], Atal Bihari Harichandan[2,*]

1. Kalinga Institute of Industrial Technology – Department of Aerospace Engineering – Bhubaneswar, India.
2. Biju Patnaik University of Technology – Centre for Undergraduate & Postgraduate Studies – Department of Mechanical Engineering – Rourkela, India.

***Correspondence author:** atal.aerodynamics@gmail.com

ABSTRACT

A numerical simulation was executed by using of ANSYS Fluent to demonstrate the effect of a Gurney flap (GF) on a National Advisory Committee for Aeronautics (NACA) 66_2-015 airfoil. The GFs are remarkable aerodynamic elements that show how a small modification to an airfoil's trailing edge can have a significant impact on performance, making them a valuable tool in the pursuit of enhanced efficiency and control in various applications with increased downforce and minimal drag penalty. The height of the flap was varied from 1% of the chord up to 3% of the chord of the airfoil, with 0.5% incremental steps. The increase in lift obtained and the subsequent penalty of increased drag were quantified in terms of percentage increase compared to the clean airfoil. As a result, the lift-to-drag ratio was found to be a net positive, with the most significant increase at a 2.5% GF height-to-chord ratio. Along with the lift augmentation, the impact of the GF on the zero-lift angle of attack, lift slope, and stall angle was investigated. Furthermore the alteration of the Kutta condition as a result of installing the GF on the airfoil. The improved aerodynamic effectiveness of airfoils using GFs is mostly observed in the motorsports and aviation sectors.

Keywords: Reynolds number; GF; Lift augmentation; Drag reduction; Lift drag ratio.

INTRODUCTION

The primary objective of an airfoil is to create lift for an aircraft to fly. Many airfoils of varied shapes have been developed to perform similar tasks in different applications. However, when the lift is not sufficient, we use lift enhancement devices, which are intended to increase the lift of any airfoil through simple modifications in it. The Gurney flap (GF) is a simple and prominent example of a lift enhancement device. It is a vertical rectangular piece placed right at the trailing edge of an airfoil to enhance its lift. The GF concept was first invented by Dan Gurney, an American motorsports racing driver and engineer. He implemented the flap on the wing of a racing car to achieve more downward force while driving at high speeds. An increase in downward force with a decrease in drag was observed. It was noted that the car could turn at higher speeds than without the GF installed. This created an interesting option for its use on airplane wings to achieve more lift.

The GF is simply a rectangular-shaped extension fitted at the trailing edge of the airfoil at a right angle to the chord on the pressure side. The height and thickness of the flap are often defined relative to the chord of the airfoil. The GF obstructs the Kutta condition, which suggests that the flow from the upper (simple) surface and lower (pressure) surface meet at the trailing edge. This creates an unusual flow behavior around the flap, including an upstream separation bubble and aft

Received: Dec 12 2023 | **Accepted:** Aug 14 2024
Section editor: Valder Steffen Jr.
Peer Review History: Single Blind Peer Review.

vortex formation as shown in Fig. 1. These flow behaviors together contribute to the increase in lift of the airfoil. Liebeck (1978) was the first person to study the use of GFs on airfoils and introduced this concept to the aerodynamics community. He conducted experimental tests in a wind tunnel with a GF height of 1.25% of the chord installed on a Newman airfoil. He observed an increase in lift with a decrease in drag. Liebeck (1978) hypothesized that the increase in lift was due to the alteration of the Kutta condition around the airfoil's trailing edge, which was later confirmed by other researchers. The Kutta condition is altered by the presence of vortices before and after the flap. A single separation bubble forms before the GF due to the obstruction of flow, and a set of two contra-rotating vortices forms at the aft of the flap which essentially pulls the flow downwards to create an upward force.

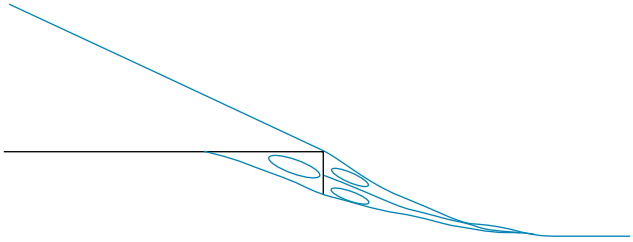

Source: Retrieved from Liebeck (1978).

Figure 1. Trailing edge flow behavior as hypothesized by Liebeck (1978).

Liu and Montefort (2007) theoretically interpreted the performance of the GF and studied the impact of increased camber on lift enhancement. They derived expressions for variations in lift and pitching moment due to GF addition on a thin airfoil. They observed that the ratio of change in lift to change in pitching moment is always constant and is equal to -4. However, their interpretation is theoretical and only accounts for the camber effect of the flap without considering the trailing edge flow behavior. Their findings also suggest that the change in lift of the airfoil is directly proportional to the square root of the GF height. Their theoretical interpretation is accurate and promising; however, its practical application might not be precise. Li *et al.* (2002) carried out experimental calculations on various GF heights and their effects on a National Advisory Committee for Aeronautics (NACA) 0012 airfoil. They observed about a 30% enhancement in maximum lift coefficient. Chen and Chen (2022) studied the effect of the GF on tiltrotor wings using numerical simulations and observed a 20.67% increase in lift coefficient with a 4% GF height. They also found that it creates a decrease in the aerodynamic performance of the airfoil, as the lift-to-drag ratio was found to decrease by 31.47% with a 4% height of the flap. Graham *et al.* (2017) studied the effects of GF thickness on airfoil performance and found out that an increase in flap thickness reduces the airfoil's performance by decreasing the pressure on the suction side and increasing the pressure on the pressure side of the airfoil. Wang *et al.* (2008) studied the mechanism and applications of GFs, along with the impact of their height, location, mounting angle, and configuration, using low-speed airfoils. They concluded that the flap is most effective when it is placed at the aft end of the airfoil, perpendicular to the chord, with a height a matching with the local boundary layer thickness.

With extensive research and study, GFs have found their use in helicopter stabilizers to lower the possibility of lift reversal, which is often the case for thick airfoils used in them. More potential uses of GFs need to be discussed considering the advantages and benefits they provide with such an uncomplicated design and manufacturing process. The study to compute and analyze an optimum GF height is of high interest. This optimum height is defined as the length of the flap that gives the maximum lift-to-drag ratio with minimal drag. The aim of this research is to study the effect of a GF on a unique asymmetrical thick airfoil, the NACA 66_2-015 airfoil. The authors will focus on varying the height of the GF from 1% of the chord up to 3%, with steps of 0.5%, to study the changes in lift, drag, and the ratio of lift-to-drag due to the GF. The optimum Gurney height will be determined by the ratio of lift-to-drag. Additionally, the formation of the contra-rotating vortices will be visualized, and the flow behavior in the vicinity of the GF will be analyzed. In addition, lift enhancement, changes in lift slope, trends in stall angle, and changes in the zero-lift angle of attack will be studied and analyzed.

Governing equations and numerical model

Governing equations

The governing equations used to solve two-dimensional (2D) fluid dynamics problems in computational fluid dynamics (CFD) are the Navier-Stokes equations of mass and momentum conservation. They include the Eqs. 1 to 3:

Continuity:
$$\frac{\partial \rho}{\partial t} + \frac{\partial (\rho u)}{\partial x} + \frac{\partial (\rho v)}{\partial y} + \frac{\partial (\rho w)}{\partial z} = 0 \quad (1)$$

X-Momentum:
$$\frac{\partial (\rho u)}{\partial t} + \frac{\partial (\rho u^2)}{\partial x} + \frac{\partial (\rho uv)}{\partial y} + \frac{\partial (\rho uw)}{\partial z} = -\frac{\partial p}{\partial x} + \frac{1}{Re}\left[\frac{\partial \tau_{xx}}{\partial x} + \frac{\partial \tau_{xy}}{\partial y} + \frac{\partial \tau_{xz}}{\partial z}\right] \quad (2)$$

Y-Momentum:
$$\frac{\partial (\rho v)}{\partial t} + \frac{\partial (\rho uv)}{\partial y} + \frac{\partial (\rho v^2)}{\partial x} + \frac{\partial (\rho vw)}{\partial z} = -\frac{\partial p}{\partial y} + \frac{1}{Re}\left[\frac{\partial \tau_{xy}}{\partial x} + \frac{\partial \tau_{yy}}{\partial y} + \frac{\partial \tau_{yz}}{\partial z}\right] \quad (3)$$

where ρ is density, t is time, (u, v, w) are component of velocity in the (x, y, z) directions, respectively, p is the pressure, Re is the Reynolds number, and τ are the components of the stress tensor. Since this is a 2D CFD problem, the z-momentum does not come into play. The Navier-Stokes equations also include the energy conservation equation, but the problem at hand deals with an isolated system with no energy transfer hence, the energy conservation is not a concern as well.

Computational setup

The computation was conducted in 2D planar and transient conditions for all calculations. The solver type was set to be pressure-based with absolute velocity formulation. It was set up with a viscous Shear Stress Transport (SST) k-Ω model. This model used the Reynolds-averaged Navier-Stokes equations, which are similar to governing equations written above with non-dimensionalization of parameters like velocities, time, viscosity, pressure, etc. The boundary conditions were set as follows: the airfoil and the top and bottom far-field were considered as walls; the upstream boundary was a velocity inlet; and the downstream boundary was a pressure outlet. This model utilizes the k-Ω model in the vicinity of the walls and the k-ε model in the open regions of the flow. This helps accurately predict the behavior of flow around the walls and the turbulent behavior of flow in the free stream. The velocity of the inlet flow was set up to achieve a Reynolds number of 3×10^5 (velocity = 29.215 m·s). The COUPLED scheme was used for pressure-velocity coupling, and a second-order implicit scheme was used for transient analysis. Reports were defined for the force report (lift coefficient) around the airfoil wall and were set as output parameters for calculating values of the lift coefficient at different angles of attack. The residual monitors were set up as accuracy of 10^{-6}. The time step size was set to 0.01 s to obtain Courant's number close to 1. Calculations were run for a time of 30 s with 3,000 time steps and a maximum of 10 iterations per time step.

Airfoil model

NACA0012

This is a symmetric airfoil with 12% chord as maximum thickness. The 2D geometry of this airfoil was imported using Airfoil Tools and modeled using its geometric coordinates. This airfoil was used to validate our calculation model and the solver's ability to yield accurate results by comparing the present results with the work of Li *et al.* (2002), who conducted a similar experiment in a laboratory using a low-speed wind tunnel.

The NACA 66_2-015 cambered airfoil has a lack of database, which is one of the reasons for selecting this airfoil. However, for validation of the computational model, an experimental calculation done previously with the GF application, had to be selected with an airfoil. For this purpose, the NACA 0012 airfoil was selected based on the past work of Li *et al.* (2002). Their experimental setup had a Reynolds number of 2×10^6 and a chord length of airfoil 1 m. For certainty, the airfoil model was subjected to a grid independence test first. The airfoil was divided into various numbers of divisions with which the grid had varying numbers of elements and nodes. The calculation was run at a 1% GF height at 0° angle of attack, and gave the results, are shown in the Table 1.

Table 1. Variation of coefficient of lift (cl) and coefficient of drag (cd) of NACA 0012 for the different grids at 1% GF height at 0° angle of attack.

No. of nodes (K)	No. of elements (K)	cl	cd
181	180	0.219709	0.0112
260	259	0.225627	0.0115
407	405	0.232476	0.0117

Source: Elaborated by the authors.

The variation in results with changes in grid fineness was not significant. Less than 6% change in the value of cl and less than 5% in the value of cd was observed when the number of elements varied from 180 K to 400 K. The model was then set similarly with the NACA 0012, and run calculations were run for GF heights ranging from 1% chord to 3% of chord. The results were validated as accurate with an error of only up to 1% for the lift coefficient, up to 7% for the drag coefficient, and up to 5% for the lift-to-drag ratio. The experimental and our numerical comparisons for the NACA 0012 airfoil are shown in Figs. 2–4. Based on the results, it was concluded that the computational setup is satisfactory for obtaining accurate data for lift, drag, and other aerodynamic parameters.

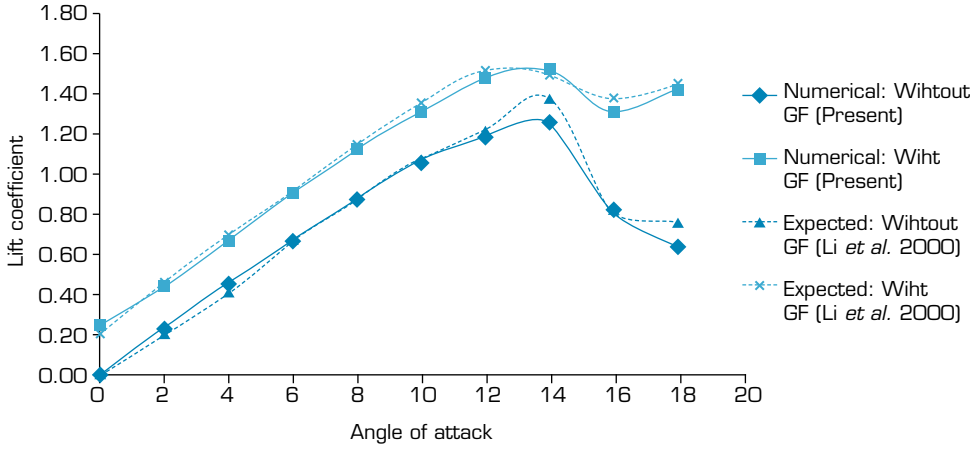

Source: Elaborated by the authors.

Figure 2. Lift curve of NACA 0012 airfoil without and with a GF of 1% h:c height (Liu and Montefort 2007).

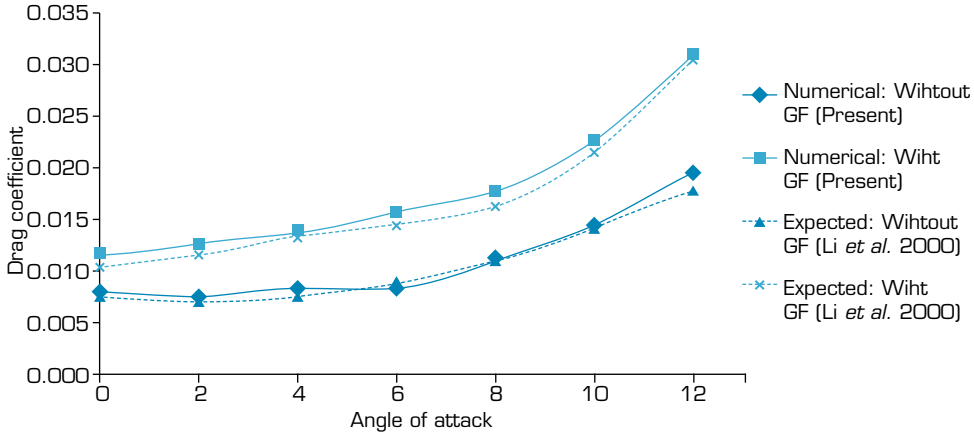

Source: Elaborated by the authors.

Figure 3. Drag curve of NACA 0012 airfoil without and with a GF of 1% h:c (Liu and Montefort 2007).

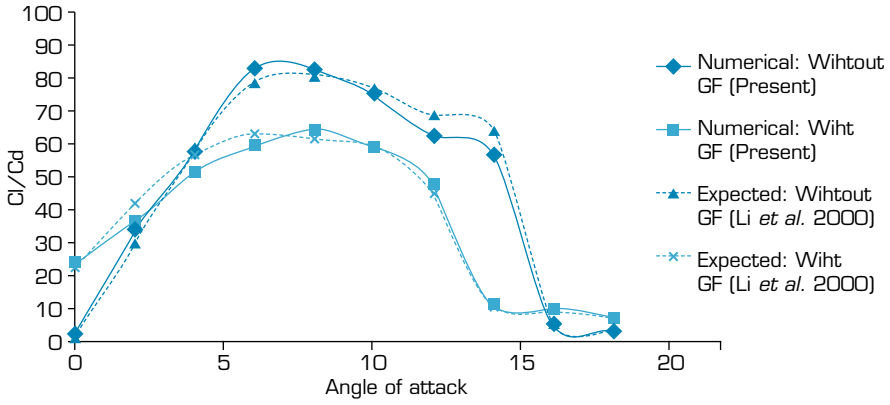

Source: Elaborated by the authors.

Figure 4. Lift-to-Drag ratio of NACA 0012 airfoil without and with GF of 1% h:c (Liu and Montefort 2007).

Gurney flap airfoil

NACA 66_2-015

This is a cambered airfoil. The geometric model is the 2D geometry of the NACA 66_2-015 cambered airfoil with a 150 mm chord length, modeled using Design Modeler in ANSYS. The data points presented in Table 2 were obtained from the Aerodynamics Lab Manual of Kalinga Institute of Industrial Technology (KIIT) University, Bhubaneshwar, India. The airfoil is unique in use, and its practical application is unclear, but the possibility of its use in submarines is suggested by some. The angle of attack of the airfoil was kept at 0°, with the rotation point at the quarter chord point, and it was set as an input parameter for calculating the flow parameters for different angles of attack later.

Table 2. Coordinates of the airfoil.

Model		
Lower Y	**X**	**Upper Y**
-0.990	0.000	0.000
-0.993	0.750	2.373
-1.054	1.125	2.977
-1.067	1.885	3.959
-0.892	3.750	5.815
-0.611	7.500	8.699
-0.412	11.250	10.933
-0.296	15.000	12.779
-0.243	22.500	15.615
-0.373	30.000	17.614
-0.644	37.500	18.986
-1.019	45.000	19.850
-1.466	52.500	20.285
-1.950	60.000	20.340
-2.437	67.500	20.050

Continue...

Table 2. Continuation.

Model		
Lower Y	**X**	**Upper Y**
-2.901	75.000	19.449
-3.304	82.500	18.547
-3.568	90.000	17.311
-3.510	97.500	15.606
-3.197	105.000	13.532
-2.694	112.500	11.202
-2.072	120.000	8.723
-1.389	127.500	6.201
-0.701	135.000	3.740
-0.149	142.500	1.550
0.000	150.000	0.000
-1.389	127.500	6.201
-0.701	135.000	3.740
-0.149	142.500	1.550
0.000	150.000	0.000

Source: Elaborated by the authors.

A vertical rectangular geometry was added at the airfoil's trailing edge to create the GF. The height of this vertical rectangle varied from 1 to 3% of chord length, corresponding to 1.50 mm, 2.25 mm, 3.00 mm, 3.75 mm, and 4.50 mm. Figure 5a and b visualize the NACA 66_2-015 without and with a GF at its trailing edge, while Fig. 5c visualizes the varying Gurney height from 1 to 3% of chord length.

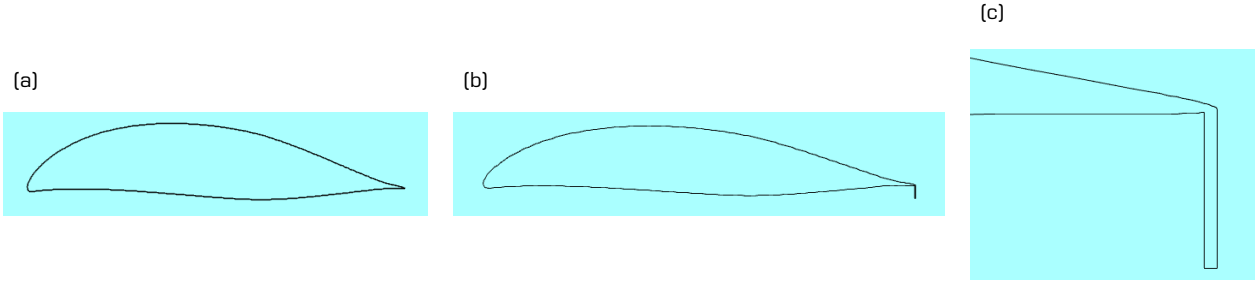

Source: Elaborated by the authors.

Figure 5. Description of the airfoil. (a) NACA 66_2-015 airfoil model; (b) NACA 66_2-015 airfoil with GF; (c) close-up view of GF at 3% h:c.

Grid generation and grid independence test

A rectangular domain was sketched around the airfoil for grid generation. The upstream and downstream boundaries were kept at 10 and 20 times of the chord length of the airfoil respectively. The top and bottom boundaries were each kept at 10 times the chord length. A structured mesh was created in the whole domain, with a very fine mesh around the airfoil and trailing edge and a coarser mesh in the far-field. Face meshing along with biased edge sizing was used. The whole airfoil was divided into 500 divisions, with a large number of divisions around the leading and trailing edges. This setting provided a fine enough mesh around

the airfoil for the desired accuracy of the calculation. The divisions around the GF were adjusted with changes in its height to obtain a finer mesh when the GF was longer. Figure 6a and b show the mesh of whole domain, and close-up mesh around the trailing edge is shown in Fig. 6c. The mesh was created using ANSYS Meshing.

Source: Elaborated by the authors.

Figure 6. Numerical grid. (a) 2D airfoil in a rectangular grid; (b) meshing in the vicinity of the airfoil; (c) close-up mesh around the GF.

To ensure the solver's accuracy, a grid independence test was conducted before proceeding with the solution. The airfoil was divided into different numbers of parts to generate the grid, which resulted in different numbers of nodes and elements. The results were reasonably close, as represented in Table 3.

Table 3. Variation of cl and cd of NACA 66_2-015 for different grids.

Domain	Airfoil divisions	No. of nodes	No. of elements	cl	cd
Very coarse mesh	100	9,030	8,800	0.3132	0.0343
Coarse mesh	300	112,780	112,000	0.4053	0.0256
Medium mesh	500	265,220	264,000	0.4099	0.0253
Fine mesh	700	481,660	480,000	0.4131	0.0249

Source: Elaborated by the authors.

Between the very coarse and coarse mesh, the difference in cl was about 29%, and the difference in cd was about 25.36%. However, the difference in cl was less than 1%, and the difference in cd was about 1.58% when the domain was changed from coarse to medium to fine mesh. This difference in cl and cd values can be further visualized in Figs. 7 and 8.

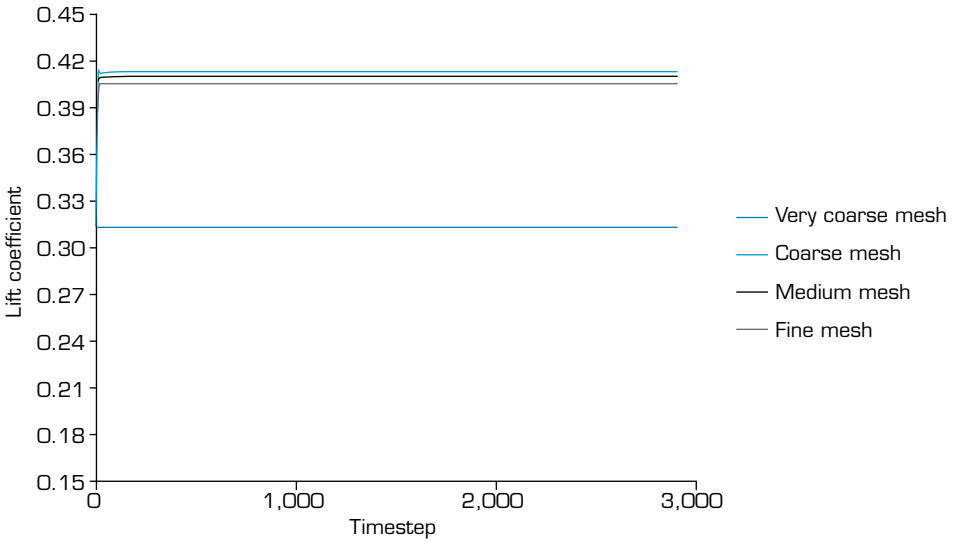

Source: Elaborated by the authors.

Figure 7. Variation of NACA 66_2-015 lift coefficient for different grids.

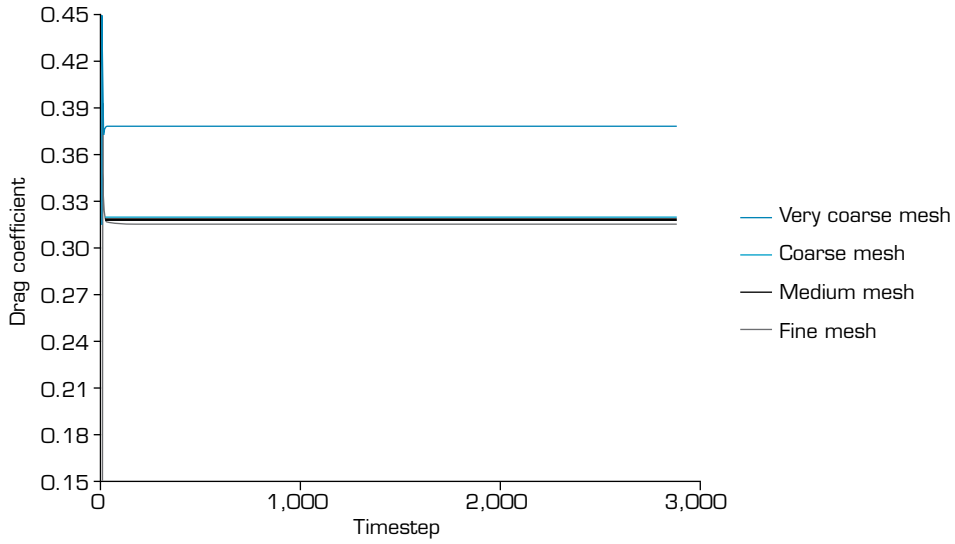

Source: Elaborated by the authors.

Figure 8. Variation of NACA 66_2-015 drag coefficient for different grids

Furthermore, due to a lack of research on the NACA 66_2-015 at this particular Reynolds number, we did not find any verified experimental data. Thus, to choose a reliable mesh, we simulated the NACA 66_2-015 airfoil from -10° to 10° angles of attack. As observed from Figs. 9 and 10, it can be seen that for every angle of attack, the values of cl and cd had significant differences when the domain was changed from very coarse to coarse mesh. However, there was no significant change in cl and cd values when changing the domain between coarse, medium, and fine mesh for every angle of attack. Therefore, medium mesh with 500 airfoil divisions was chosen as a reliable mesh domain for further simulations.

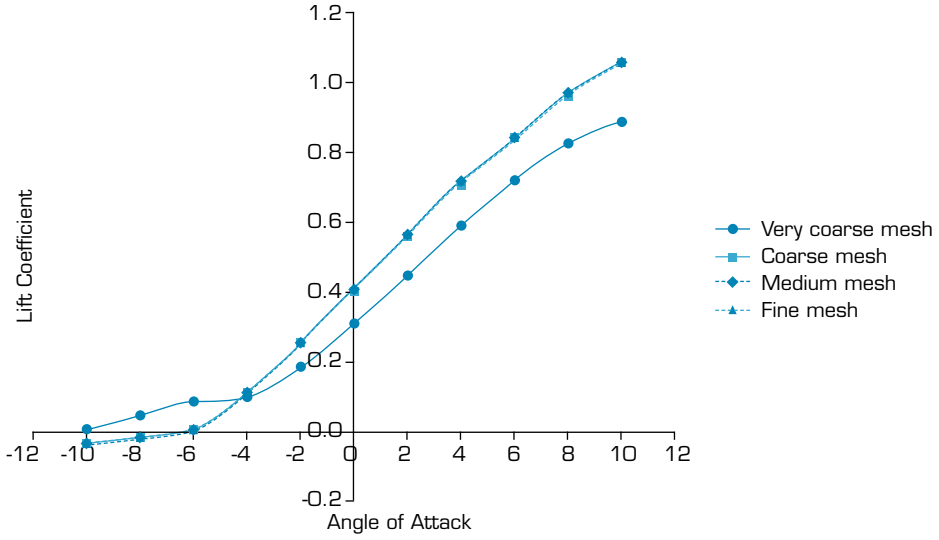

Source: Elaborated by the authors.

Figure 9. Lift curve of NACA 66_2-015 for different angles of attack and different grids.

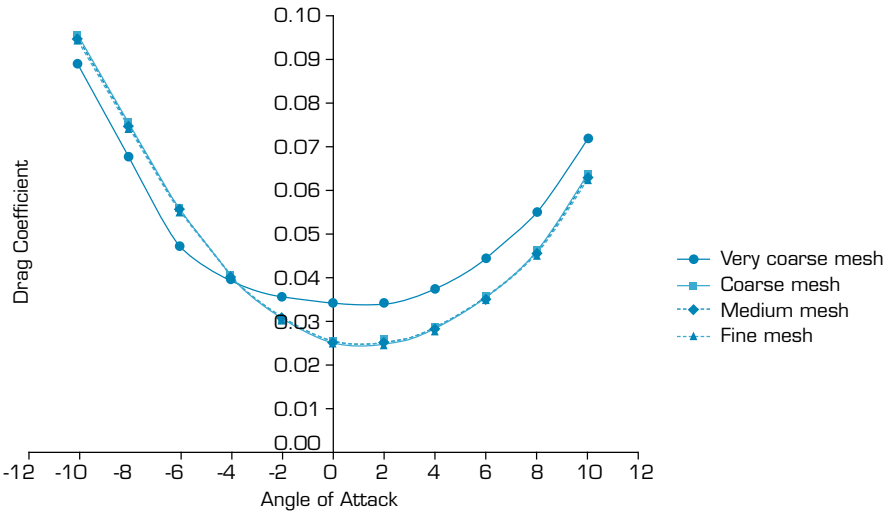

Source: Elaborated by the authors.

Figure 10. Drag curve of NACA 66_2-015 for different angles of attack and different grids.

RESULTS AND DISCUSSION

All calculations were done with a velocity of 29.215 m·s yielding a Reynolds number of 3×10^5 based on the reference chord length, which is 0.15 m. The study was conducted on a clean airfoil and 1, 1.5, 2, 2.5, and 3% h:c GF airfoils. The lift curves, drag curves, and ratio of lift-to-drag for each configuration were calculated. Velocity contours and streamlines of flow with and without the GF were visualized using CFD-Post, and the behavior of the low was in good agreement with the hypothesis of Liebeck (1978).

Evaluation of GF performance on aerodynamic characteristics

The lift slope, drag slope, and ratio of lift-to-drag plotted in Figs. 11–13 depict the magnitude of increase in the lift coefficient, the drag coefficient, and the ratio of lift-to-drag for every angle of attack with an increase in the height of the GF. The highest increase in maximum lift coefficient, i.e., 48.69%, and the highest increase in maximum drag coefficient, i.e., 55.95%, were observed when the GF height was kept at 3% h:c height. Meanwhile, the highest increase in the lift-to-drag coefficient, i.e., 140.68%, was observed at 2.5% h:c height. Thus, a 2.5% GF was determined to be the optimum height for better aerodynamic efficiency. Lift at zero-degree angle of attack was increased by almost 160% when the GF height was kept at 3% h:c. The effect of the GF was satisfactory based on the observations of the lift curve, the drag curve, and the ratio of lift-to-drag curve.

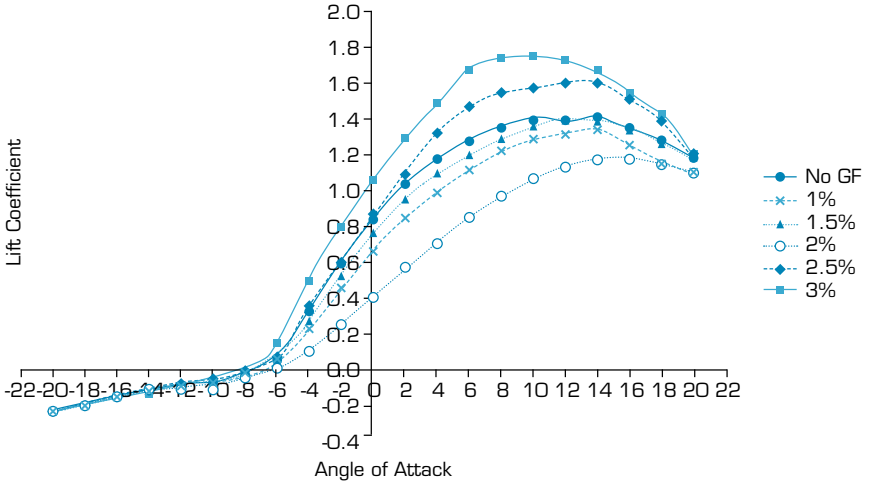

Source: Elaborated by the authors.

Figure 11. Lift curve of NACA 66_2-015 airfoil with and without GF.

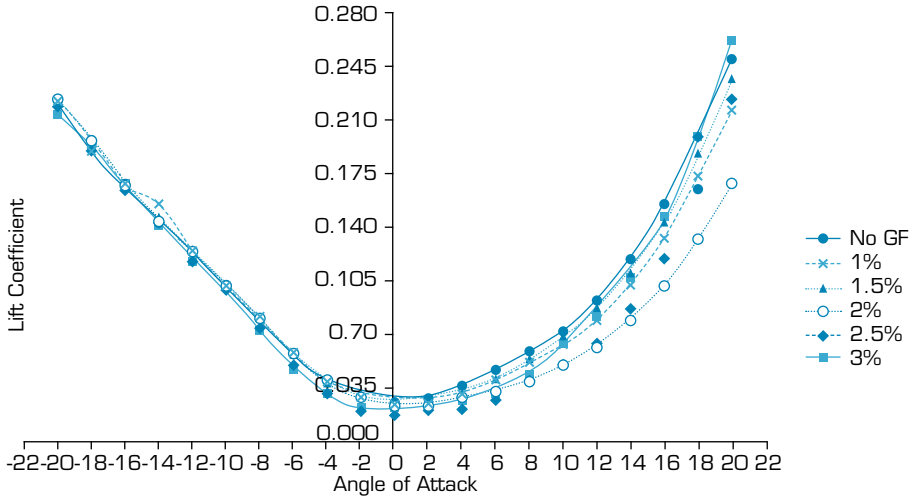

Source: Elaborated by the authors.

Figure 12. Drag curve of NACA 66_2-015 airfoil with and without GF.

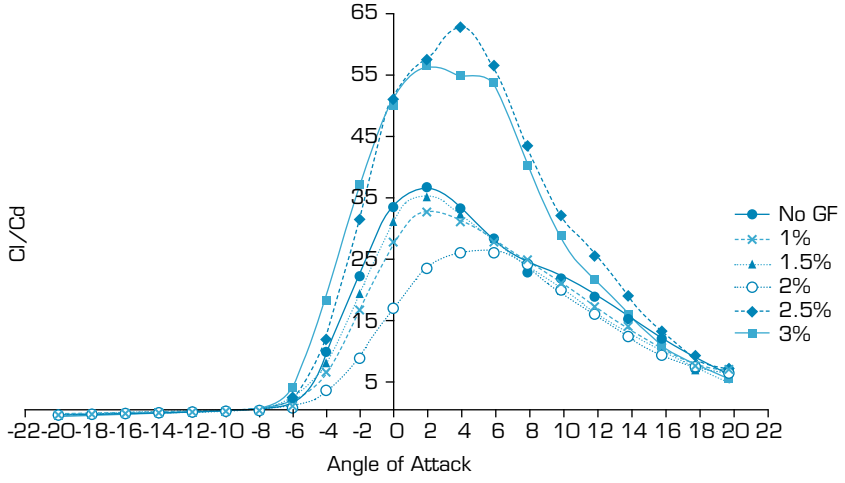

Source: Elaborated by the authors.

Figure 13. Lift-to-drag ratio of NACA 66_2-015 airfoil with and without GF.

Velocity contours

The effect of the GF in the velocity contour around the trailing edge is of interest in this subsection. The secret behind the lift augmentation of the GF is its ability to alter the Kutta condition at the trailing edge and shift it towards the end of the GF. This phenomenon is best observed when the velocity contours of a clean airfoil and airfoils with GFs of different heights are compared. The velocity contours of the airfoil with different GF heights at 0º angle of attack are shown in Fig. 14. The authors claim that as the height of the GF increases, the flow is essentially pulled downwards towards the GF. The GF creates a downward momentum of fluid around it, which causes this pull-down effect to happen. The flow separation bubble on the upper surface of the airfoil, which was distinct in the clean airfoil, slowly disappeared as the height of the GF increased, due to the increase in the camber effect. The contra-rotating vortices grow larger and larger as the height of the flap increases. This effect is obvious in its nature, but it can be noted that the flow is turned downwards due to these vortices. Therefore, the larger the height of the GF, the larger the vortices, the greater the downward momentum of fluid, and the higher the lift.

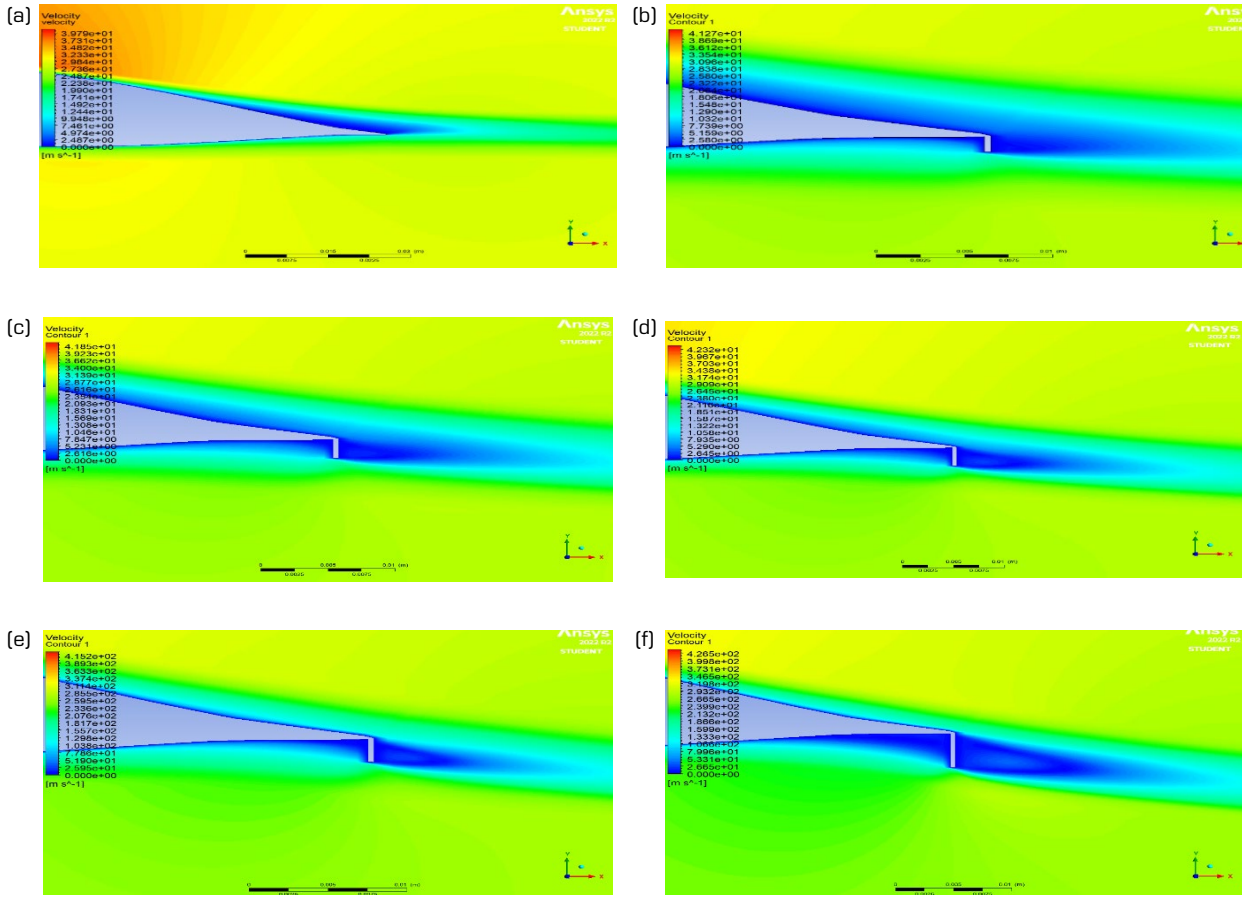

Source: Elaborated by the authors.

Figure 14. Velocity contours around trailing edge of airfoil with GF and without GF at 0º angle of attack. (a) airfoil without GF; (b) 1% h:c; (c) 1.5% h:c; (d) 2% h:c; (e) 2.5% h:c; (f) 3% h:c.

Trailing edge flow behavior

To more clearly visualize the behavior of the flow at the trailing edge or around the GF, streamlines of the flow were generated around the trailing edge for the clean airfoil and the airfoil with a 3% GF height. The streamlines in Fig. 15 show that for the clean airfoil, the Kutta condition is followed, and the flow passes smoothly through the trailing edge; a small separation bubble is formed where the flow attempts to separate. For the airfoil with the GF, the flow around the trailing edge behaves differently. The entire flow is pulled downwards towards the end of the GF. A small separation bubble is formed in front of the GF, which cancels out some of the drag created by the flap itself. In addition to that, a pair of contra-rotating vortices are seen in Fig. 16 behind the flap, which are responsible for the downward momentum of fluid and the increase in lift. This behavior of flow around the trailing edge is in good agreement with the hypothesis of Liebeck (1978) and has been verified by various researchers thereafter.

Aerodynamic performance of NACA 66_2-015 with GF

The effect of the GF is not limited to an increment in the lift coefficient, the drag coefficient, and the ratio of lift-to-drag, or trailing edge flow behavior altercations; it also affects the stall angle of the airfoil, the zero-lift angle of attack, and more. Calculations were performed for angles of attack from -20^0 to 20^0 with a step of 2 degrees. From the data obtained, the authors interpolated the zero-lift angle of attack. The maximum lift coefficient and stall angles were calculated based on the observed data points only. The lift slope was calculated by considering the straight part of the lift curve for each configuration of the GF. The aerodynamic parameters of the studied airfoil with the GF are presented in Table 4.

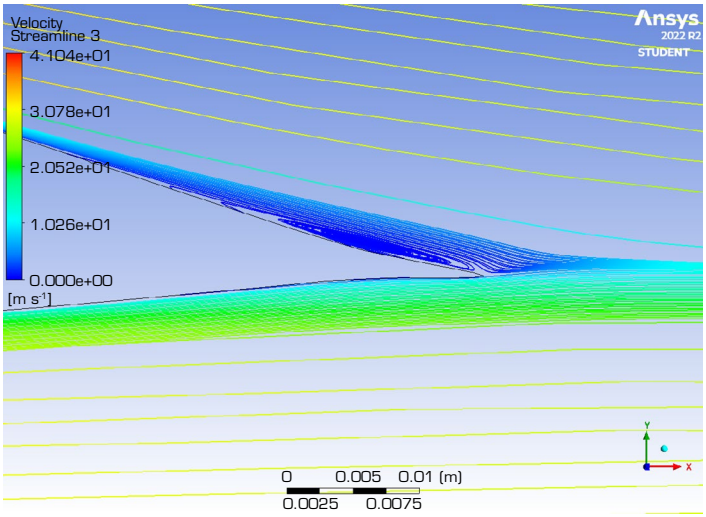

Source: Elaborated by the authors.

Figure 15. Streamline around the trailing edge of the airfoil without GF at 0º angle of attack.

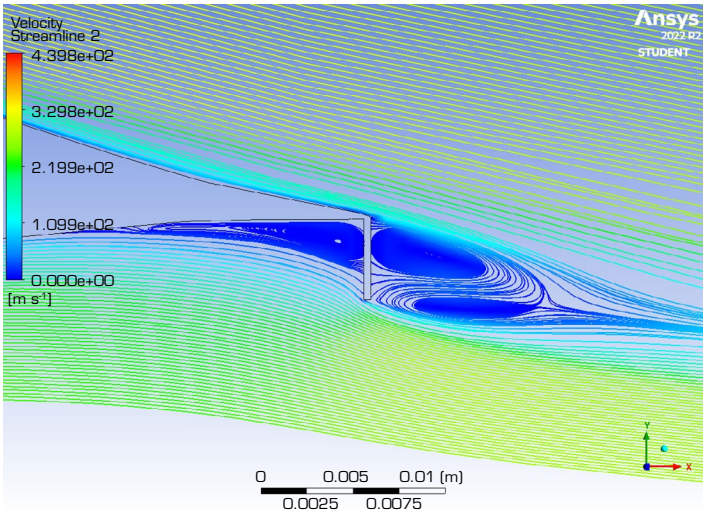

Source: Elaborated by the authors.

Figure 16. Streamline around the trailing edge of the airfoil with a GF of height 3% h:c at 0º angle of attack.

Table 4. Effect of GF height on aerodynamic parameters of NACA 66_2-015.

Configuration	c_l (max)	α_{stall} (°)	αl_0 (°)	c_l, α (rad^{-1})	c_d (max)	c_l/c_d (max)
No GF	1.180	16	-6.12	3.919	0.199	26.088
1% h:c	1.347	14	-7.03	5.122	0.222	32.324
1.5% h:c	1.401	12	-7.07	5.306	0.229	35.078
2% h:c	1.412	12	-7.14	6.566	0.230	36.607
2.5% h:c	1.613	12	-7.68	6.744	0.222	62.791
3% h:c	1.754	10	-7.97	7.334	0.264	56.409

Source: Elaborated by the authors.

The increase in the values of cl(max), cd(max), and cl/cd(max) is evident from the lift curve, drag curve, and ratio of lift-to-drag curve previously discussed, and the exact values of the data are presented here. The stall angle of attack of the airfoil slowly decreases as the GF height increases, and the lift curve was also seen to shift to the left. Furthermore, the zero-lift angle also follows the same trend of decreasing with the increase in GF height. These changes in zero-lift angles of attack are not so significant but are worth noting in terms of the effect the GF has on these parameters. The effect of GF height on the lift slope is proportional. The lift slope increases as the height of the GF increases, which can also be seen in the lift curve in Fig. 6.

Conclusion and scope for future works

The present study has concluded that a GF is a device with ideal mechanical simplicity, which can provide a large magnitude of lift augmentation for an asymmetrical thick airfoil. The increment in lift obtained was significant, quantitatively 14.14, 18.71, 19.65, 36.72, and 48.69% for GF's height/chord ratio of 1, 1.5, 2, 2.5, and 3% relative to an clean airfoil. With the increase in the lift, it also penalized the performance by an increase in drag, which was 31.08, 41.03, 47.97, 31.47, and 55.95%, respectively, for the same height/chord ratios. As a result, the net increase in the lift-to-drag ratio obtained was 23.9, 34.46, 40.32, 140.68, and 116.22%, respectively. This proved that a 2.5% GF height provided the optimum advantage in lift augmentation. The velocity profile of flow around the GF's trailing edge was visualized to provide the flow with a net downward momentum as the height of the GF increased. Streamlines or particle tracing of flow around the trailing edge geometry without and with the GF visualized the difference in flow patterns that were created due to the setup of the flap. A separation bubble and two contra-rotating vortices were observed, which are responsible for the lift augmentation. It was noticed that as the flap height increases the maximum lift increases and the stall angle decreases. The zero-lift angle of attack also decreases with the increase in flap height and finally the slope of the lift curve increases as the flap height increases.

The effect of GF height on other aerodynamic parameters, such as pitching moment, as well as the effect of GF width, angle, position, and orientation, can be studied in future works. The most effective study of the GF would be to determine the optimum height, width, and position of the GF for a particular application by considering the advantage of lift augmentation and accounting for the disadvantageous reduction in the lift-to-drag ratio.

CONFLICT OF INTEREST

Nothing to declare.

AUTHORS' CONTRIBUTION

Conceptualization: Mandal B, Gupta RK, and Adhikari A; **Methodology:** Mandal B, Gupta RK, and Adhikari A; **Software:** Mandal B, Gupta RK, and Adhikari A; **Validation:** Mandal B, Gupta RK, and Adhikari A; **Formal analysis:** Mandal B, Gupta RK, and Adhikari A; **Investigation:** Mandal B, Gupta RK, and Adhikari A; **Resources:** Mandal B, Gupta RK, and Adhikari A; **Data Curation:** Mandal B, Gupta RK, and Adhikari A; **Writing - Original Draft:** Mandal B, Gupta RK, and Adhikari A; **Writing - Review & Editing:** Das BN and Harichandan AB; **Supervision:** Das BN and Harichandan AB; **Final approval:** Harichandan AB.

DATA AVAILABILITY STATEMENT

Data sharing is not applicable.

FUNDING

Not applicable.

ACKNOWLEDGMENTS

Not applicable.

REFERENCES

Chen H, Chen B (2022) Lift enhancement of tiltrotor wing using a Gurney flap. Int J Aerosp Eng (1):1-9. https://doi.org/10.1155/2022/1245484

Graham M, Muradian A, Traub LW (2017) Experimental study on the effect of Gurney flap thickness on airfoil performance. J Aircr 55(2):897-903. https://doi.org/10.2514/1.C034547

Li Y, Wang J, Zhang P (2002) Effects of Gurney flaps on a NACA0012 airfoil, flow turbulence and combustion. Flow Turbul Combust 68(1):27-39. https://doi.org/10.1023/A:1015679408150

Liebeck RH (1978) Design of subsonic airfoils for high lift. J Aircr 15(9)547-561. https://doi.org/10.2514/3.58406

Liu T, Montefort J (2007) Thin-airfoil theoretical interpretation for Gurney flap lift enhancement. J Aircr 44(2):667-671. https://doi.org/10.2514/1.27680

Wang JJ, Li YC, Choi KS (2008) Gurney flap – Lift enhancement, mechanisms and applications. Prog Aerosp Sci 44(1):22-47. https://doi.org/10.1016/j.paerosci.2007.10.001